Aalto University

OPEN ACCESS

This is an electronic reprint of the original article.
This reprint may differ from the original in pagination and typographic detail.

Imala, Mikk-Markus; Naar, Hendrik; Tabri, Kristjan; Romanoff, Jani

Toward the application of the layer-wise displacement theory in passenger ships—a quasi-static response

Published in:
Mechanics of Advanced Materials and Structures

DOI:
10.1080/15376494.2022.2103859

Published: 01/01/2023

Document Version
Publisher's PDF, also known as Version of record

Published under the following license:
CC BY-NC-ND

Please cite the original version:
Imala, M.-M., Naar, H., Tabri, K., & Romanoff, J. (2023). Toward the application of the layer-wise displacement theory in passenger ships—a quasi-static response. *Mechanics of Advanced Materials and Structures*, *30*(22), 4698-4710. https://doi.org/10.1080/15376494.2022.2103859

This material is protected by copyright and other intellectual property rights, and duplication or sale of all or part of any of the repository collections is not permitted, except that material may be duplicated by you for your research use or educational purposes in electronic or print form. You must obtain permission for any other use. Electronic or print copies may not be offered, whether for sale or otherwise to anyone who is not an authorised user.

Mechanics of Advanced Materials and Structures

ISSN: (Print) (Online) Journal homepage: https://www.tandfonline.com/loi/umcm20

Toward the application of the layer-wise displacement theory in passenger ships—a quasi-static response

Mikk-Markus Imala, Hendrik Naar, Kristjan Tabri & Jani Romanoff

To cite this article: Mikk-Markus Imala, Hendrik Naar, Kristjan Tabri & Jani Romanoff (2023) Toward the application of the layer-wise displacement theory in passenger ships—a quasi-static response, Mechanics of Advanced Materials and Structures, 30:22, 4698-4710, DOI: 10.1080/15376494.2022.2103859

To link to this article: https://doi.org/10.1080/15376494.2022.2103859

© 2022 The Author(s). Published with license by Taylor & Francis Group, LLC

Published online: 01 Aug 2022.

Submit your article to this journal

Article views: 791

View related articles

View Crossmark data

Full Terms & Conditions of access and use can be found at
https://www.tandfonline.com/action/journalInformation?journalCode=umcm20

MECHANICS OF ADVANCED MATERIALS AND STRUCTURES
2023, VOL. 30, NO. 22, 4698–4710
https://doi.org/10.1080/15376494.2022.2103859

Taylor & Francis
Taylor & Francis Group

ORIGINAL ARTICLE

OPEN ACCESS Check for updates

Toward the application of the layer-wise displacement theory in passenger ships—a quasi-static response

Mikk-Markus Imala[a], Hendrik Naar[a], Kristjan Tabri[a], and Jani Romanoff[b]

[a]Department of Civil Engineering and Architecture, Tallinn University of Technology, Tallinn, Estonia; [b]Department of Mechanical Engineering, Aalto University, Helsinki, Finland

ABSTRACT

This paper introduces an application of the layer-wise displacement theory for response analysis of multilayer ship girders. Quadrilateral, 6-node finite membrane elements are used for which 8 displacement degrees of freedom at corners, and 4 shear strain degrees of freedom at mid-side nodes, are defined. This approach enables accurate estimates of the shear strain between adjacent layers with different stiffness. A simple cantilever beam, non-uniform stepped girder with constant layer stiffness, and uniform girder with varying stiffness is used in the validation analysis. An excellent agreement between the fine mesh finite element model and the proposed model is observed.

ARTICLE HISTORY
Received 1 March 2022
Accepted 17 July 2022

KEYWORDS
Quasi-static structural response; layer-wise displacement theory; higher-order beam theory; finite element method; girder analysis

1. Introduction

Today, a variety of marine structures such as tankers and cargo and single-deck ships are sufficiently accurately assessed at the preliminary stage with the simplest forms of beam analysis that describe the hull girders as a single slender beam; reviews of common structural rules for bulkers and tankers are presented by Yao [1], Sumi [2]. However, recent trends in structural design for ships have been introducing shear-weak and long, stepped, superstructures, changing the typical transfer of shear stresses to a more complex phenomenon as described by Naar et al. [3], Shi and Gao [4, 5], Romanoff et al. [6] and Morshensholuk and Khedmati [7]. Due to this complexity, today, the most widely used method for solving passenger ship response is the three-dimensional (3 D) finite element method (FEM) [8]. In addition to the high computational solution time, global finite element models are time-consuming to create. Therefore, analytical methods or coarse mesh finite element models are preferred in the early design stage where design time is limited, as described by Avi [9]. Mathematical analysis of ship hull girders was first introduced by A. N. Krylov at the start of the 20th century [10]. The hull and superstructure interaction methods using the beam theories were first introduced by Crawford et al. [11] by considering the shear and vertical coupling in a two-beam system through additional stress resultants (internal shear and vertical forces between beams). A similar approach is introduced by Bleich et al. [12], where the stresses in prismatic beams in a vertically coupled two-beam system were considered. A review paper of non-classical continuum mechanics application in marine engineering by Romanoff et al. [13] suggested that the response of a shear-weak superstructure does not follow internally a typical shear force diagram that the entire hull-girder experiences. The paper offers two possible solutions. The first would be, to exploit non-classical continuum mechanics, and to add a micropolar correctional factor to a Timoshenko beam to estimate micropolar moments over the height of the beam, allowing the layerwise, internal variation, of shear stress resultants within the hull girder height and length. The second would exploit classical continuum mechanics such as a layer-wise formulation for the beam. The first of such layer-wise formulations was the linear Coupled Beam presented by Naar et al. [3]. The method uses shear and vertical coupling between layers to evaluate the response of multideck passenger ships. Toming et al. [14] investigated the interaction of hull and superstructure using the Coupled Beam method by implementing a piece-wise approach, where layers of a multideck ship are divided into beam segments for which the structural behavior is individually described using continuous coordinate functions to describe local structural discontinuities. Non-linear Coupled Beam theory was consequently presented by Naar [15] and Morshensholuk and Khedmati [7] to assess hull girder limit-states accounting for non-linearities arising from local buckling or yielding.

Today, most beam theory applications within the marine industry utilize the Euler-Bernoulli or Timoshenko beam theory [16] which either neglects or oversimplifies the shear behavior. The extensions to these practices in the marine structures' community could exploit the developments from

CONTACT Mikk-Markus Imala mikk-markus.imala@taltech.ee Department of Civil Engineering and Architecture, Tallinn University of Technology, Tallinn, Estonia.

© 2022 The Author(s). Published with license by Taylor & Francis Group, LLC
This is an Open Access article distributed under the terms of the Creative Commons Attribution-NonCommercial-NoDerivatives License (http://creativecommons.org/licenses/by-nc-nd/4.0/), which permits non-commercial re-use, distribution, and reproduction in any medium, provided the original work is properly cited, and is not altered, transformed, or built upon in any way.

the solid mechanics community. Levinson [17], Bickford [18], Rehfield and Murthy [19], Krishna Murty et al. [20], Bhimaraddi and Chandrashekhara [21], and Baluch et al. [22] have presented parabolic shear deformation theories for beams using a higher variation of axial displacement in terms of height coordinate. Ghugal and Sharma [23] have proposed a variationally consistent hyperbolic shear deformation theory for thick beams and further refined the theory in [24]. A higher-order shear deformation theory was introduced by Reddy [25], where the in-plane displacement fields follow a third-order polynomial. Many of these beam theories have been extended to layer-wise theories, that can be applied when analyzing composite laminates or structures. These could be also applied in ships with shear-weak and stepped, long superstructures interacting with more rigid hulls deforming according to EB- or Timoshenko beam theories. An excellent overview of multilayer theories was published by Carrera [26]. The review focuses on the theories setting assumptions for the description of displacements in the cross-section's normal direction and the stresses in the thickness direction. To achieve interlaminar continuity, an equilibrium for the stresses in the thickness direction is assumed in Lekhnitskii multilayered theory [27], Ambartsumian multilayered theory [28] and the multilayered theory based on the Reissner mixed variational theorem [29]. Additionally, these theories have made several integral assumptions for a layer-wise approach such as the equilibrium of displacements in adjacent surfaces and third-order displacement field definitions used, for example, by Toledano and Murakami [30]. The layer-wise displacement theory of Reddy [31] assumes a displacement field that uses an independent approximation of variables in the thickness direction from in-plane approximations. A generalization of the layer-wise displacement theory is presented in Reddy's later research [32], where the approach is applied to beams. Carrera unified formulation (CUF) is an approach that generalizes polynomial expansion methods for beams, plates, and shells including laminated and multi fields loadings that has the potential to be applied in marine technology applications as shown by Rehan [33] for simple ship hull girders and global hull girder responses in terms of displacements. The potential of this formulation in the passenger ship context is providing the means to create refined higher-order models where the specific approximation type being used and the order to which the approximation is expanded are considered as the parametrically free problem inputs. The CUF has found many applications in both statics [34–37] and dynamics [38–40] on beams, plates and shells undergoing small and application with large displacements [41–43]. These works include originally classical papers [44–46] and recently also expansions to non-classical structural models and use-cases [47–49]. In the present paper context, the interest is in the early works which focus on beam stress analysis and related finite element formulations [34, 36, 37, 50] as the application to passenger ships calls for both and especially increased accuracy on the stress assessment.

This article includes reference data presented by Pagani et al. [37] that includes a novel hierarchical Legendre polynomial expansion model in addition to referencing analysis data using Taylor expansion models and classical beam theories. These advancements in beam theories have the potential for applications within the marine structures' community, in the analysis of complex hull girders such as in passenger ships.

This paper aims to bridge the gap between layer-wise theories typically used for composite laminates and extend their application toward the marine industry. The layer-wise method developed in this paper lends the assumptions for interlaminar continuity of displacements from the classical layer-wise displacement theory while introducing a novel membrane element definition that achieves the desired stress behavioral capabilities. In marine structures, in-plane shear stress over the height of a ship is often non-continuous due to the differences in plate thicknesses, secondary stiffening, and non-linear responses due to different failure modes in layers (e.g. local buckling, yielding). This characteristic is achieved with a novel finite element definition that in addition to in-plane displacements at element corner nodes, includes hybrid shear strain degrees of freedom (DOFs) in mid-side nodes in the ship height direction. The representation of the shear strain component values at the coordinates of the corner nodes as mid-side node DOFs enables an uncoupled description of shear stresses between vertically adjacent elements, which is necessary to describe the non-continuous nature of shear stress in adjacent structures, where topology or material properties vary. Axial displacement of the membrane element is approximated with a third-order polynomial through the ship height direction, whereas for the displacement in the ship height direction linear approximation is accurate enough. This formulation allows using large elements that can accurately approximate the displacements and normal and shear stresses that are of fundamental importance in the design of complex passenger ship hull girders, where the layers are thin, yet shear stresses can be significant and non-continuous. Thus, computational accuracy and efficiency are enhanced in comparison to the alternative 4- or 8-noded membrane elements. The presented method is validated in two stages. Firstly, a comparative analysis is performed on a layered cantilever beam for which the results are compared to an analysis performed by Pagani et al. [37]. In the article, the authors compared the results of various Carrera's Unified Formulation (CUF) models using hierarchical Legendre polynomial expansions and Taylor expansions. Secondly, the numerical results are compared between the presented method and finite element analysis using commercially available software with stepped and shear-weak hull girder models.

2. Higher-order coupled beam theory

2.1. Definition of variables

The method is described for a quadrilateral membrane element defined in the Cartesian coordinate system. The x-axis is aligned with the length l, and the y-axis with the height h, of the element. The finite element is defined with 6 nodes.

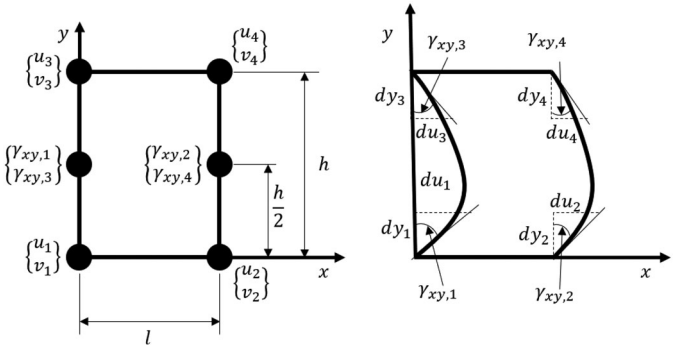

Figure 1. Beam element in the Cartesian coordinate system and explanation of shear strain DOFs.

The corner nodes, 1–4, are complemented with mid-side nodes in the y-direction, as shown in Figure 1.

DOFs in a membrane element, see Figure 1, are as follows:

- $u_1, \ldots, u_4$—displacement in x-axis direction at corner nodes
- $v_1, \ldots, v_4$—displacement in y-axis direction at corner nodes
- $\gamma_{yx,1}, \ldots, \gamma_{yx,4}$—shear strain due to horizontal shifting at the locations of the corner nodes.

As the stiffness properties of the layers in the passenger ship height direction often vary, it is necessary to uncouple shear strains between layers. Thus, the shear strain DOF is expressed in mid-side nodes leaving these variables uncoupled between adjacent elements in the ship height direction in the global stiffness matrix.

Ship structures are traditionally considered to act as thin-walled structures due to the high ratio between in-plane and thickness dimensions. Although significant i.e. for a single deck vibration analysis or a buckling analysis of a singular stiffened panel, out-of-plane behavior has little effect on the global response of a passenger ship.

2.2. Definition of the displacement field

The in-plane displacement fields $u(x,y)$ and $v(x,y)$ of the developed membrane element are individually expressed as a combination of polynomial functions in y direction as:

$$u(x_0,y) = A_{u,1}y^3 + B_{u,1}y^2 + C_{u,1}y + D_{u,1}, \tag{1}$$

$$v(x_0,y) = A_{v,1}y + B_{v,1}. \tag{2}$$

Equations (1) and (2) use the following relations to solve the polynomial equations at $x = 0$ for constants $A_{u,1}, B_{u,1}, C_{u,1}, D_{u,1}$ and $A_{v,1}, B_{v,1}$:

$$\begin{cases} u(0,0) = u_1 \\ \dfrac{\partial u}{\partial y}(0,\ 0) = \gamma_{yx,1} \\ u(0,h) = u_3 \\ \dfrac{\partial u}{\partial y}(0,\ h) = \gamma_{yx,3}, \end{cases} \tag{3}$$

$$\begin{cases} v(0,0) = v_1 \\ v(0,h) = v_3. \end{cases} \tag{4}$$

After inserting values of constants to Eqs. (1) and (2), regrouping for DOFs shown in Figure 1, and adding first-order approximations $\phi_1(x)$, $\phi_2(x), \xi_1(y), \xi_2(y)$, displacement fields are described as a linear combination of shape functions and DOFs:

$$\begin{aligned} u(x,y) = {} & \psi_1(y)\phi_1(x)u_1 + \psi_1(y)\phi_2(x)u_3 + \psi_2(y)\phi_1(x)\gamma_{xy,1} \\ & + \psi_2(y)\phi_2(x)\gamma_{xy,3} + \psi_3(y)\phi_1(x)u_2 + \psi_3(y)\phi_2(x)u_4 \\ & + \psi_4(y)\phi_1(x)\gamma_{xy,2} + \psi_4(y)\phi_2(x)\gamma_{xy,4}, \end{aligned} \tag{5}$$

$$\begin{aligned} v(x,y) = {} & \xi_1(y)\phi_1(x)v_1 + \xi_1(y)\phi_2(x)v_3 + \xi_2(y)\phi_1(x)v_2 \\ & + \xi_2(y)\phi_2(x)v_4, \end{aligned} \tag{6}$$

where

$$\begin{cases} \psi_1(y) = \dfrac{h^3 - 3hy^2 + 2y^3}{h^3} \\ \psi_2(y) = \dfrac{h^2y - 2hy^2 + y^3}{h^2} \\ \psi_3(y) = \dfrac{3hy^2 - 2y^3}{h^3} \\ \psi_4(y) = \dfrac{y^3 - hy^2}{h^2}, \end{cases} \tag{7}$$

$$\begin{cases} \xi_1(y) = 1 - \dfrac{y}{h} \\ \xi_2(y) = \dfrac{y}{h}, \end{cases} \tag{8}$$

$$\begin{cases} \phi_1(x) = 1 - \dfrac{x}{l} \\ \phi_2(x) = \dfrac{x}{l}. \end{cases} \tag{9}$$

or in vector form as:

$$u(x,y) = \{N\}^T\{u\}, \tag{10}$$

$$v(x,y) = \{V\}^T\{v\}. \tag{11}$$

where $\{N\}$ and $\{V\}$ are vectors of shape functions and $\{u\}$ and $\{v\}$ are vectors including nodal DOFs in axial and in the ship height direction as presented in Eqs. (5) and (6).

Ship structures are often composed of stiffened panels for which the orthotropic approach is needed as it enables modeling the stiffened panel as a homogeneous plate structure. The in-plane normal and shear strains are expressed as:

$$\begin{aligned} \begin{Bmatrix} \varepsilon_{xx} \\ \varepsilon_{yy} \\ 2\varepsilon_{xy} \end{Bmatrix} &= \begin{Bmatrix} \dfrac{\partial u(x,y)}{\partial x} \\ \dfrac{\partial v(x,y)}{\partial y} \\ \dfrac{\partial u(x,y)}{\partial y} + \dfrac{\partial v(x,y)}{\partial x} \end{Bmatrix} \\ &= \begin{Bmatrix} \left\{\frac{\partial N}{\partial x}\right\}^T\{u\} \\ \left\{\frac{\partial V}{\partial y}\right\}^T\{v\} \\ \left\{\frac{\partial N}{\partial y}\right\}^T\{u\} + \left\{\frac{\partial V}{\partial x}\right\}^T\{v\} \end{Bmatrix}. \end{aligned} \tag{12}$$

2.3. Expression of potential energy

For an orthotropic material, where material axes (x_1, x_2, x_3) is coincident with coordinate axes (x, y, z), stress components according to the generalized Hooke's law are:

$$\begin{Bmatrix} \sigma_{xx} \\ \sigma_{yy} \\ \sigma_{xy} \end{Bmatrix} = \begin{bmatrix} C_{11} & C_{12} & 0 \\ C_{12} & C_{22} & 0 \\ 0 & 0 & C_{66} \end{bmatrix} \begin{Bmatrix} \varepsilon_{xx} \\ \varepsilon_{yy} \\ 2\varepsilon_{xy} \end{Bmatrix} \tag{13}$$

where C_{ij} are the elastic stiffnesses:

$$C_{11} = \frac{E_1}{(1-\nu_{12}\nu_{21})},\ C_{22} = \frac{E_2}{(1-\nu_{12}\nu_{21})},\ C_{12} = \nu_{12}C_{22},\ C_{66} = G_{12}. \tag{14}$$

Here, E_1 and E_2 are Young's moduli in the x and y directions, respectively, G_{12} is the in-plane shear modulus and ν_{12} and ν_{21} are Poisson ratios described as:

$$\nu_{21} = \nu_{12}\frac{E_2}{E_1}. \tag{15}$$

The potential strain energy equation for an orthotropic membrane element is written as:

$$\begin{aligned} \Pi &= \frac{1}{2}\int_0^l\int_A (\sigma_{xx}\varepsilon_{xx} + \sigma_{yy}\varepsilon_{yy} + \sigma_{xy}2\varepsilon_{xy})dAdx - \int_0^l p_y v(x,y)dx \\ &= \frac{1}{2}\int_0^l\int_A \left(C_{11}\varepsilon_{xx}^2 + C_{12}\varepsilon_{yy}\varepsilon_{xx} + C_{12}\varepsilon_{xx}\varepsilon_{yy} + C_{22}\varepsilon_{yy}^2 + C_{66}(2\varepsilon_{xy})^2\right)dAdx \\ &- \int_0^l p_y v(x,y)dx, \end{aligned} \tag{16}$$

for which the first variation of potential energy is:

$$\begin{aligned} \delta\Pi = &\int_0^l\int_A \left(\frac{\partial\delta u}{\partial x}C_{11}\frac{\partial u}{\partial x}\right)dAdx + \int_0^l\int_A \left(\frac{\partial\delta v}{\partial y}C_{22}\frac{\partial v}{\partial y}\right)dAdx \\ &+ \int_0^l\int_A \left(\frac{\partial\delta u}{\partial x}C_{12}\frac{\partial v}{\partial y}\right)dAdx + \int_0^l\int_A \left(\frac{\partial\delta v}{\partial y}C_{12}\frac{\partial u}{\partial x}\right)dAdx \\ &+ \int_0^l\int_A \left(\frac{\partial\delta u}{\partial y}C_{66}\frac{\partial u}{\partial y}\right)dAdx + \int_0^l\int_A \left(\frac{\partial\delta u}{\partial y}C_{66}\frac{\partial v}{\partial x}\right)dAdx \\ &+ \int_0^l\int_A \left(\frac{\partial\delta v}{\partial x}C_{66}\frac{\partial u}{\partial y}\right)dAdx + \int_0^l\int_A \left(\frac{\partial\delta v}{\partial x}C_{66}\frac{\partial v}{\partial x}\right)dAdx \\ &- \int_0^l p_y\delta v(x,y)dx = 0, \end{aligned} \tag{17}$$

where

$$\delta u = \{\delta a\}^T\{N\}, \tag{18}$$

$$\delta v = \{\delta b\}^T\{V\}. \tag{19}$$

$\{\delta a\}$ and $\{\delta b\}$ are vectors of variations of arbitrary constants. By substituting Eqs. (10), (11), (18), and (19) into Eq. (17) finite element equations become:

$$K11_{i,j} = \int_0^l\int_A \left(\left(\frac{d}{dx}N_iC_{11}\frac{d}{dx}N_j\right) + \left(\frac{d}{dy}N_iC_{66}\frac{d}{dy}N_j\right)\right)dAdx \tag{20}$$

$$K12_{i,j} = \int_0^l\int_A \left(\left(\frac{d}{dy}N_iC_{66}\frac{d}{dx}V_j\right) + \left(\frac{d}{dx}N_iC_{12}\frac{d}{dy}V_j\right)\right)dAdx \tag{21}$$

$$K21_{i,j} = \int_0^l\int_A \left(\left(\frac{d}{dx}V_iC_{66}\frac{d}{dy}N_j\right) + \left(\frac{d}{dy}V_iC_{12}\frac{d}{dx}N_j\right)\right)dAdx \tag{22}$$

$$K22_{i,j} = \int_0^l\int_A \left(\left(\frac{d}{dx}V_iC_{66}\frac{d}{dx}V_j\right) + \left(\frac{d}{dy}V_iC_{22}\frac{d}{dy}V_j\right)\right)dAdx \tag{23}$$

$$F_i = \int_0^l p_yV_idx \tag{24}$$

The first variation of potential energy in Eq. (17) can be written using finite element equations from Eqs. (20) to (24) as:

$$\begin{aligned} \delta\Pi = &\{\delta a\}^T([K11]\{u\} + [K12]\{v\}) \\ &+ \{\delta b\}^T([K21]\{u\} + [K22]\{v\} - \{F\}) \\ = &\ 0. \end{aligned} \tag{25}$$

As $\{\delta a\}$ and $\{\delta b\}$ are vectors of arbitrary constants, the first variation can only equal to zero if the two components in brackets in Eq. (25) are individually equal to zero, thus:

$$\begin{bmatrix} [K11] & [K12] \\ [K21] & [K22] \end{bmatrix} \begin{Bmatrix} u \\ v \end{Bmatrix} = \begin{Bmatrix} 0 \\ F \end{Bmatrix}. \tag{26}$$

The vector of constants in Eq. (26) is rearranged and node-wise grouped as shown in Figure 1, where every node has 2 DOFs to facilitate the formulation of the global stiffness matrix and global loading vector as:

$$[K]\begin{Bmatrix} u_1 \\ v_1 \\ u_2 \\ v_2 \\ \gamma_{xy,1} \\ \gamma_{xy,2} \\ \gamma_{xy,3} \\ \gamma_{xy,4} \\ u_3 \\ v_3 \\ u_4 \\ u_4 \end{Bmatrix} = \{F\} \tag{27}$$

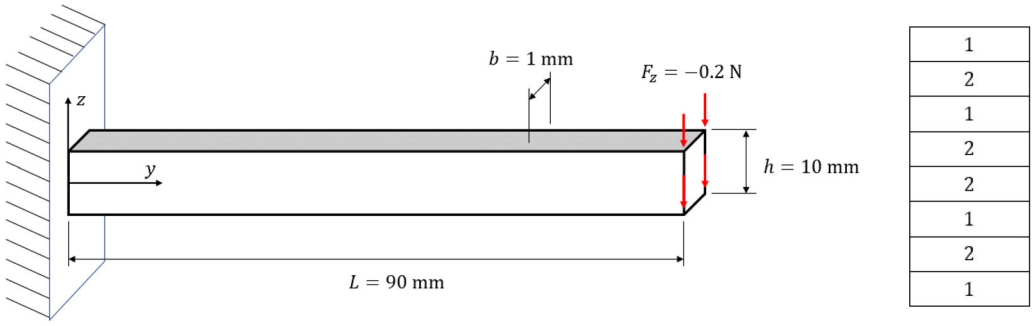

Figure 2. Cantilever beam model and layer configuration presented by Pagani et al. [37].

where $[K]$ and $\{F\}$ are the rearranged stiffness matrix and external loading vector respectively.

3. Models used for analysis

3.1. Cantilever beam model

Proof of concept analysis is performed on a cantilever beam model for which 8 separated layers defined with two different sets of material properties were incorporated. The reference data values for the analysis and the topological properties of the cantilever beam are presented in Pagani et al. [37]. The model in Figure 2 illustrates a thin cantilever beam with a varying configuration of layers to clearly distinguish the effects of changing material properties at layer transitions. The materials used to define the layers have identical transversal elastic modulus ($E_T = 1$ GPa), shear modulus ($G = 0.5$ GPa) and possion ratio ($\nu = 0.25$). Longitudinal elastic modulus is $E_{L1} = 30$ GPa for material 1 and $E_{L2} = 5$ GPa for material 2, see Figure 2 for layer configuration. The Poisson ratio and shear modulus is assumed to be constant in all directions. The cantilever beam is loaded at the free end from each cross-section corner with four equal loads summing up to $F_z = -0.2$ N. The model is located in a Cartesian coordinate system, where the y-axis is coincident with the longitudinal direction and the z-axis is coincident with the transversal direction of the model. See Figure 2 for the cantilever beam model and the layer configuration.

The cantilever beam is defined with 72 elements for the application of the presented theory, where every layer consists of 9 elements in the longitudinal direction resulting in 340 DOFs in total.

3.2. Hull girder models

To illustrate the layerwise application of the developed finite element in a marine context two case studies are considered. These are selected from Toming et al. [14] from which two simplified ship hull girders were considered,[1] one representing a stepped beam with uniform stiffness in layers and another representing a uniform beam with varying stiffness in layers.

The stepped beam model consists of three adjacent membrane sections in the ship height direction with varying lengths. Each membrane section is described with a single layer of elements for the Quad6 and coarse mesh Quad4 models consisting of a total of 120 elements. Additionally, the Quad6 fine mesh model has been included in stepped beam model analysis to more accurately describe the corner effects by separating each membrane section into three layers of elements for which $h = 1000$ mm, thus consisting of a total of 360 elements. The fine mesh finite element (FE) model, used for comparison, consists of 9300 Quad4 membrane elements with dimensions of 200×200 mm, see Figure 3(a) for the model dimensions and the FE models. The model for the uniform beam with varying layer stiffness consists of three adjacent membrane sections with equal lengths, where the upper layers have large openings, which lower the overall stiffness of the structure and alter stress distributions. For the Quad6 and coarse mesh Quad4 models, the membrane sections with openings are both divided into three individual layers as the openings are described with offsets from beam surfaces consisting of a total of 520 elements. The fine mesh FE model consists of 23,000 Quad4 membrane elements with dimensions of 150×150 mm, see Figure 3(b) for the dimensions and the coarse FE model and Figure 3(d) for comparative size of the applied fine mesh. The elastic foundation has been used as boundary conditions for FE-models as it provides an accurate representation of a hull girder bending in waves, see Figure 3(c) for boundary principles.

Identical sinusoidal loading has been applied to all models to the bottom surface nodes excluding the elastic foundation elements as shown in Figure 4. The distributed loading is calculated as:

$$p(x) = p_0 * \cos\left(\frac{2\pi x}{L}\right), \tag{28}$$

where p_0 is load amplitude taken as 60N/mm, L is the total length of the model taken as 60 m. Material properties for elastic modulus and Poisson's ratio are used for FE membrane models: $E = 210$GPa, and $\nu = 0.3$ respectively. FE-analysis was performed using NX Nastran and FEMAP Academic version for Quad4 membrane models and Mathcad 15 software for Quad6 membrane models.

[1]The Cases B and C from the paper from the paper represent stepped beam with constant stiffness in layers and uniform beam with varying stiffness in layers respectively. We exploit here the latter wording for physical insight.

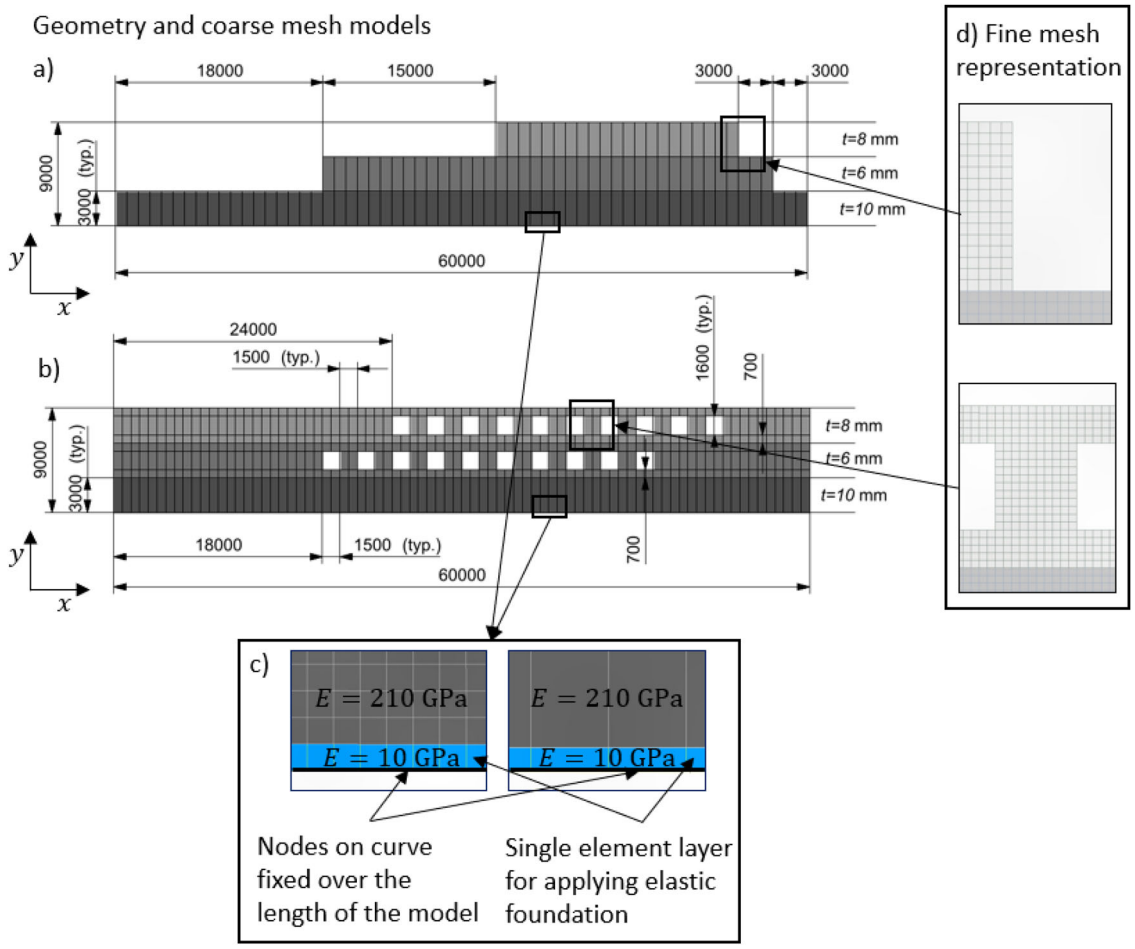

Figure 3. Geometry and FE plate models for (a) stepped beam with uniform layer stiffness and (b) uniform beam with varying layer stiffness, (c) principles of applying elastic foundation, and (d) detail views showing the comparative size of the used fine mesh.

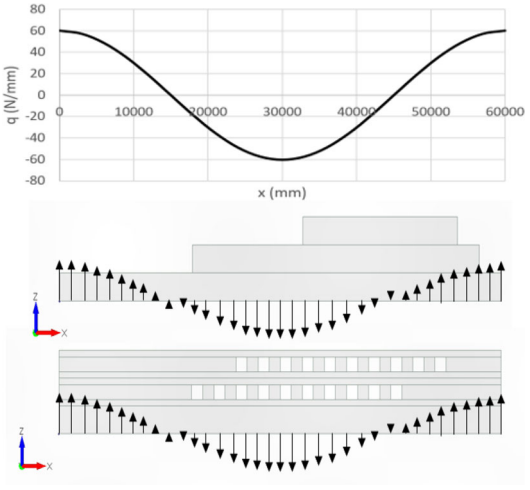

Figure 4. The applied distributed loading to the stepped beam with uniform stiffness and uniform beam with varying stiffness between layers.

4. Results

4.1. Cantilever beam model

The analysis performed for the 8-layer cantilever beam in [37] involved expressing the transversal distribution of normal and shear stress at the cross-section $y = L/2$. The data from Figure 11 from the referenced article is lumped together depending on the coincidence of the results between the used methods. For the normal stress analysis, the Euler-Bernoulli beam method (EBBM), Timoshenko beam method (TBM), and the results for the 6-th order Taylor expansion model (TE N6) were lumped as well as the presented hierarchical Legendre expansion models (8HL2, 8HL4, 8HL6, 8HL8) with various n-th order ($n = 2, 4, 6, 8$) were lumped together due to highly coincident values. The layerwise theory presented in this article shows extremely coincident results to the hierarchical Legendre expansion models. These methods are distinguished by the ability to accurately describe the non-continuous stress behavior at the layer transitions compared to the analytical method, classical beam theory, and Taylor expansion model values, see Figure 5.

For shear stress comparison, hierarchical Legendre expansion model results (8HL2, 8HL4, 8HL6, 8HL8) are lumped, whereas the 6-th and 9-th order Taylor expansion models (TE N6, TE N9) produce highly different results. The presented layerwise theory results are similarly in good agreement with the results of the hierarchical Legendre expansion models, see Figure 6.

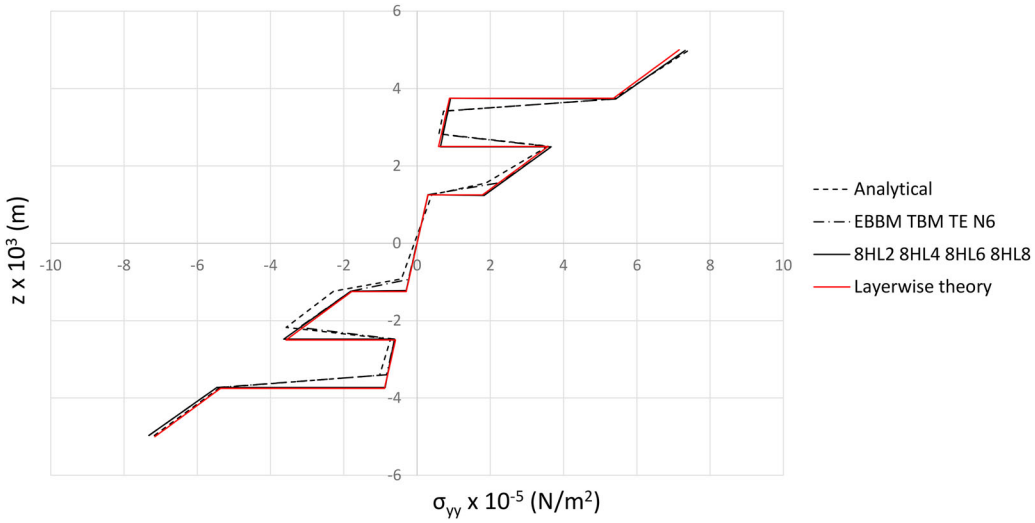

Figure 5. Transversal distribution of normal stresses at $y = L/2$ for the presented layerwise method and analyzed theories in [37].

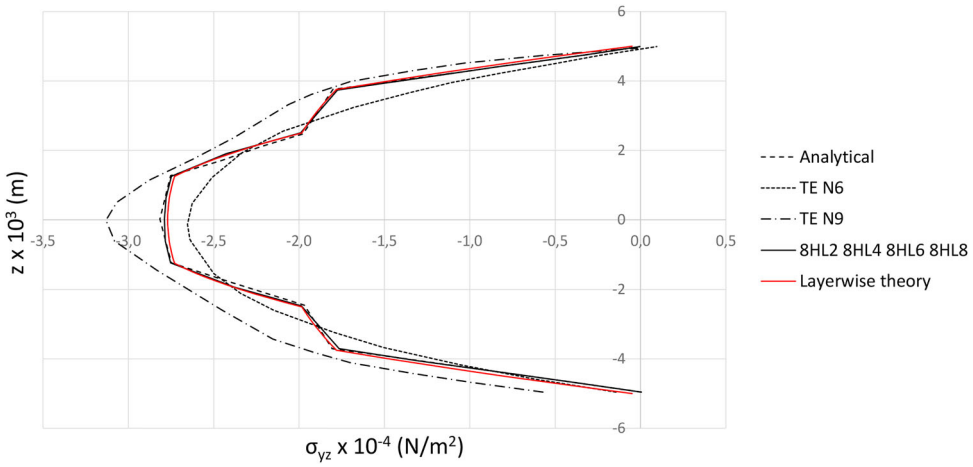

Figure 6. Transversal distribution of shear stresses at $y = L/2$ for the presented layerwise method and analyzed theories in [37].

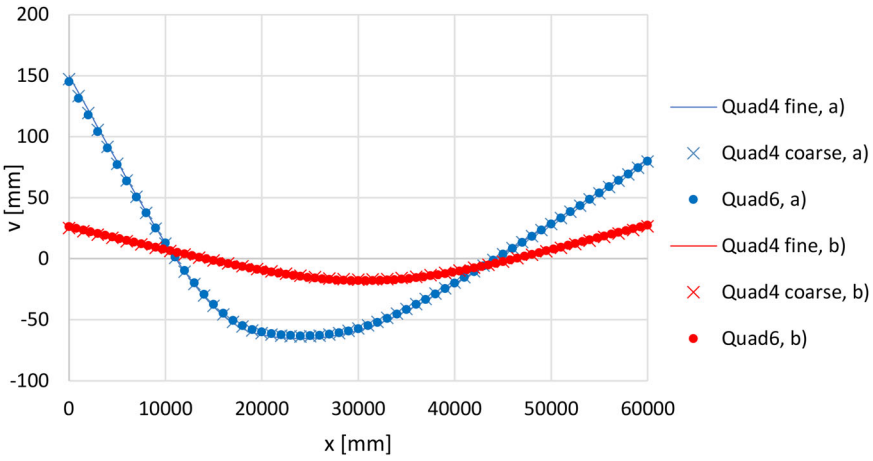

Figure 7. Comparison of deflections: (a) stepped beam, (b) unified beam with varying layer stiffnesses.

4.2. Hull girder models

Figure 7 presents the vertical displacements of different models. The global behavior of the models is in an agreement between the fine mesh and the Quad-6 mesh developed in this paper, and the coarse Quad-4 mesh.

4.2.1. Stress results for the stepped beam

For the stepped beam, the normal stresses have been analyzed in horizontal planes at $y = \frac{H}{3} = 3000\,\text{mm}$ and $y = \frac{2H}{3} = 6000\text{mm}$ and the top layer at $y = H = 9000\text{mm}$, along girder length, see Figure 8. The stress results are in good agreement with the fine mesh results, however, peak stress

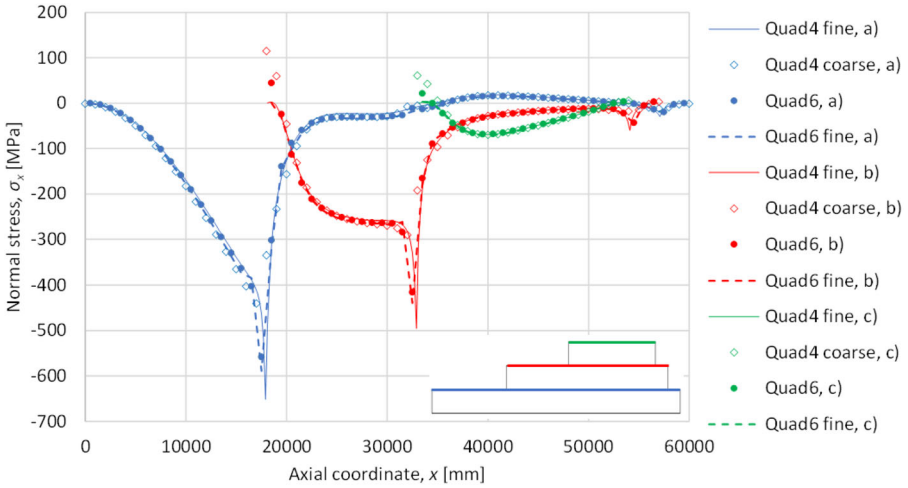

Figure 8. Longitudinal distribution of normal stress at (a) y = H/3 = 3000 mm, (b) y = 2H/3 = 6000 mm, (c) y = H = 9000 mm.

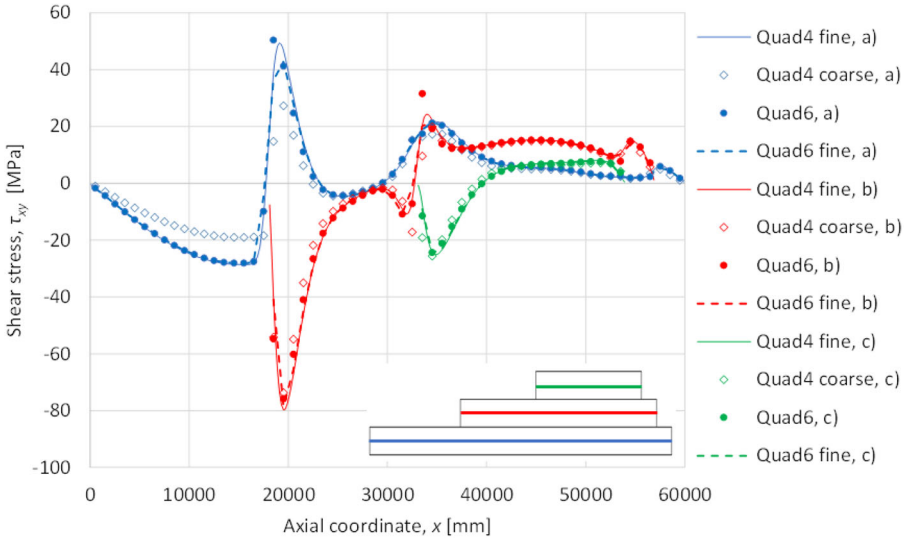

Figure 9. Longitudinal distribution of shear stress at (a) y = H/6 = 1500 mm, (b) y = H/2 = 4500 mm, (c) y = 5/6H = 7500 mm.

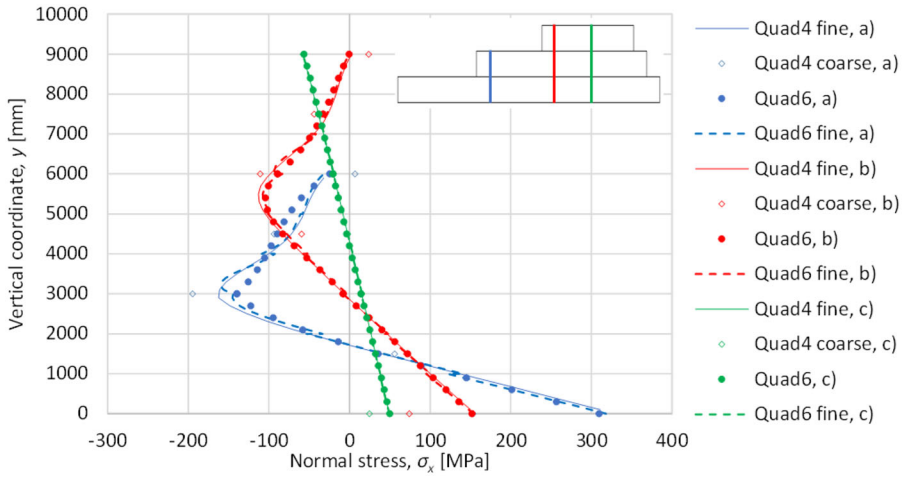

Figure 10. Normal stress, σ_x, in the stepped beam at (a) x = 19,500 mm, (b) x = 34,500 mm, (c) x = 43,500 mm.

values are generally underestimated with Quad6 and coarse mesh Quad4 model, Quad 6-results being considerably more accurate. In addition, stress decay at the vertical boundary edges is more accurately described with Quad6. When finer Quad-6 mesh is utilized the results are in excellent agreement with the fine mesh results.

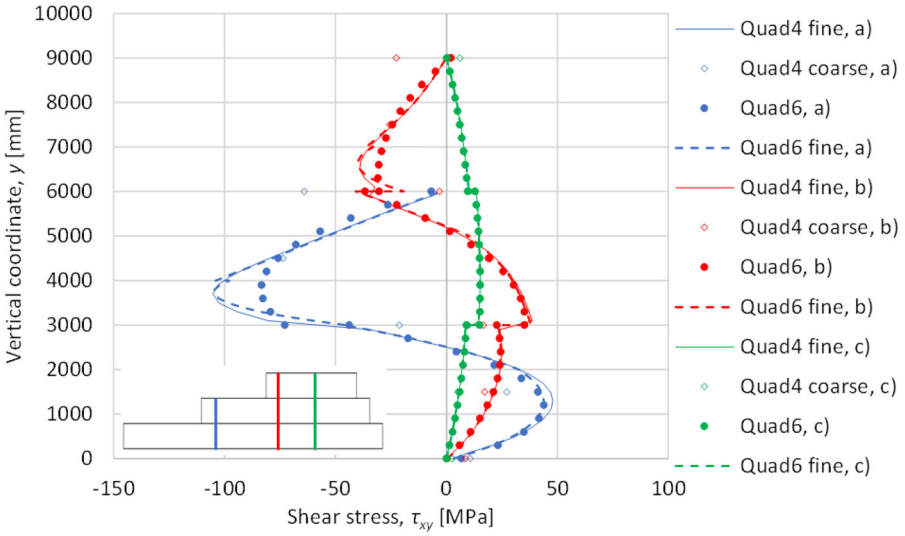

Figure 11. Shear stress of the stepped beam (a) x = 19,500 mm, (b) x = 34,500 mm, (c) x = 43,500 mm.

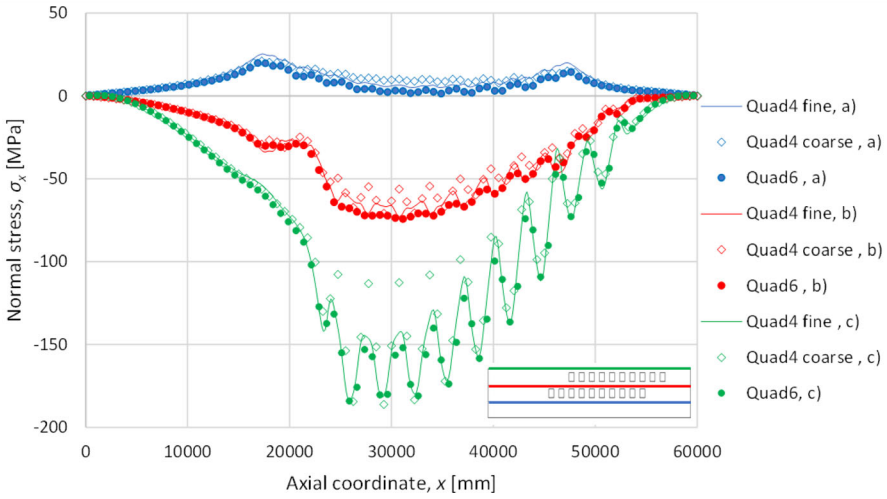

Figure 12. Longitudinal distribution of normal stress, σ_x, at (a) y = H/3 = 3000 mm, (b) y = 2H/3 = 6000 mm, (c) y = H = 9000 mm.

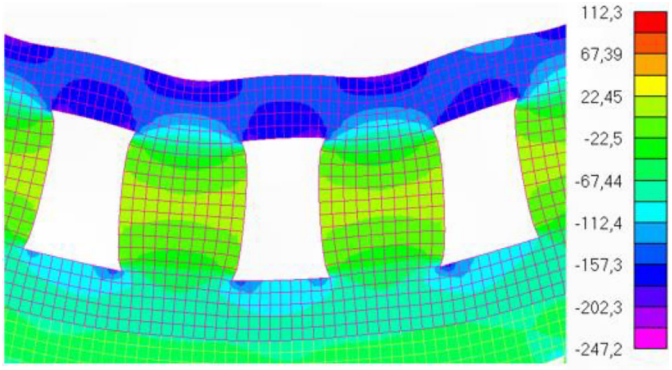

Figure 13. Local bending response in low bending stiffness areas for fine Quad4 element model of the uniform beam with varying layer stiffness.

The longitudinal distribution of shear stresses is analyzed in the middle layers of the layers at $y = \frac{H}{6} = 1500\text{mm}$, $y = \frac{H}{2} = 4500\,\text{mm}$ and $y = \frac{5}{6H} = 7500\,\text{mm}$, see Figure 9. In general Quad6 element models and fine mesh, model results are in agreement, whereas as coarse Quad4 element underestimates the stresses, especially at the discontinuities. Again Quad6 mesh models show excellent performance in comparison to fine mesh when element size is decreased.

Cross-sections for analyzing the transversal distribution of normal stresses, σ_x, have been chosen such that both linear and higher-order distribution of stresses through the height of the girder can be seen. For the stepped beam with uniform stiffness in layers, cross-sections close to discontinuities at $x = \frac{L}{3.08} \approx 19,500\,\text{mm}$ and $x = \frac{L}{1.74} \approx 34,500\,\text{mm}$ and linearly behaving cross-section at $x = \frac{L}{1.38} \approx 43,500\,\text{mm}$ are chosen.

Vertical distribution of normal stress shows excellent agreement in all selected sections between Quad6 element model and fine mesh, with finer Quad6-mesh increasing the accuracy. In comparison, the fine mesh model does not agree with the coarse Quad4 mesh model at the places where significant discontinuities occur. This highlights the need for Quad6 element formulation, see Figure 10.

As an extension to the investigation on normal stresses, the distribution of shear stresses in the vertical direction shows highly corresponding results for fine mesh and coarse Quad6. Decreasing the Quad6 element size again improves

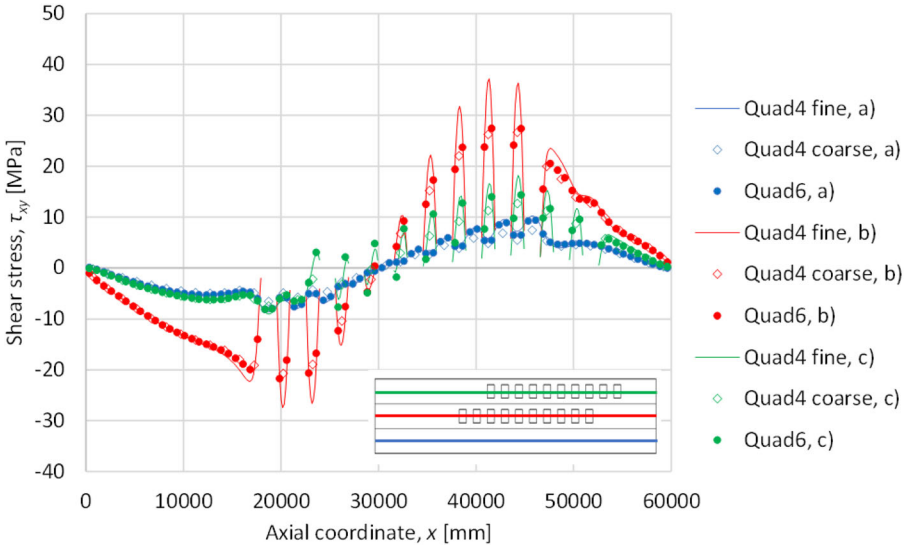

Figure 14. Longitudinal distribution of shear stress at (a) z = 1500 mm, (b) z = 4500 mm, (c) z = 7500 mm.

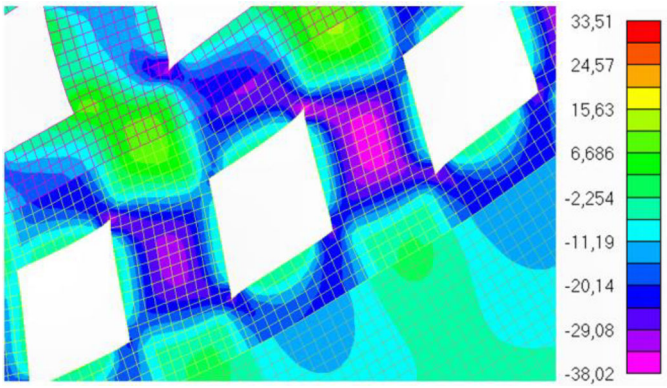

Figure 15. Local shear response in low shear stiffness areas for the fine Quad4 element model of the uniform beam with varying layer stiffness.

the agreement, while the same cannot be concluded from the Quad4 coarse mesh, see Figure 11. As in the case of normal stresses, this justifies the use of Quad6-formulation.

4.2.2. Stress results for the uniform beam with varying layer stiffness

The axial distribution of normal stresses, σ_x, in the uniform beam with varying layer stiffness shows overall good correspondence between the fine-, Quad6- and Quad4-meshes, see Figure 12. The Quad6 element model describes the oscillation of stress highly accurately when compared to the fine mesh model, while the coarse Quad4 element model overestimates the oscillation amplitude at the midspan region in planes y = 2H/3 and y = H. The oscillating normal stresses form most prominently in the top surface as openings introduce areas along the free edges, where bending stiffness is lowered and secondary shear strain occurs. In a global bending situation, the free edge geometry of openings is deformed and the structures on top of openings provide an opposite local bending response, see Figure 13.

When the shear stresses are observed in the middle of the layers, the Quad6 and Quad 4 results are in agreement with the fine mesh results, except for the peak values, see Figure 14. As Figure 15 shows in the vicinity of openings, the traction-free stress conditions cannot be accurately described with the Quad6 or Quad4 element models. These discrepancies can be addressed by decreasing element dimensions in stress-critical areas in sub-models.

For the unified beam with varying stiffness in layers, cross-sections close to discontinuities at $x = \frac{L}{1.38} \approx 43,875$ mm, in the middle of a shear weak section at $x = \frac{L}{2.42} \approx 24,750$ mm and linearly behaving cross-section at $x = \frac{L}{4.10} \approx 14,625$ mm are chosen. Transversal distributions of normal stresses for the unified beam with varying stiffness in layers show excellent agreement between Quad6 and fine mesh models, see Figure 16. The Quad6 element model describes normal stress as a continuous function throughout the cross-sections as well as the effects of openings in high detail. Results for the coarse Quad4 element model are more scattered, especially for the cross-sections with openings.

In the same way, the shear stresses in the ship height direction are in agreement between the Quad6 and fine mesh models, while the coarse Quad 4 element model has difficulties modeling the fine mesh results, see Figure 17.

5. Concluding remarks

This paper introduced an application for the layer-wise displacement theory to evaluate displacements and stress distributions in layer-wise models with changing material and topological parameters as are present in the marine industry in passenger ships with long superstructures. This application creates a need for a 6-node finite membrane element with two displacement DOFs in corner nodes and two shear strain DOFs in mid-side nodes of transverse edges. Similar to classical 4-node membrane elements, these developed elements can be used to describe complex membrane structures. This approach generates a realistic distribution of normal and shear stresses in the hull girder. We have presented two case studies for the developed element to express the applicability in areas of discontinuous stepped layers, areas of openings or shear-weak sections and areas of

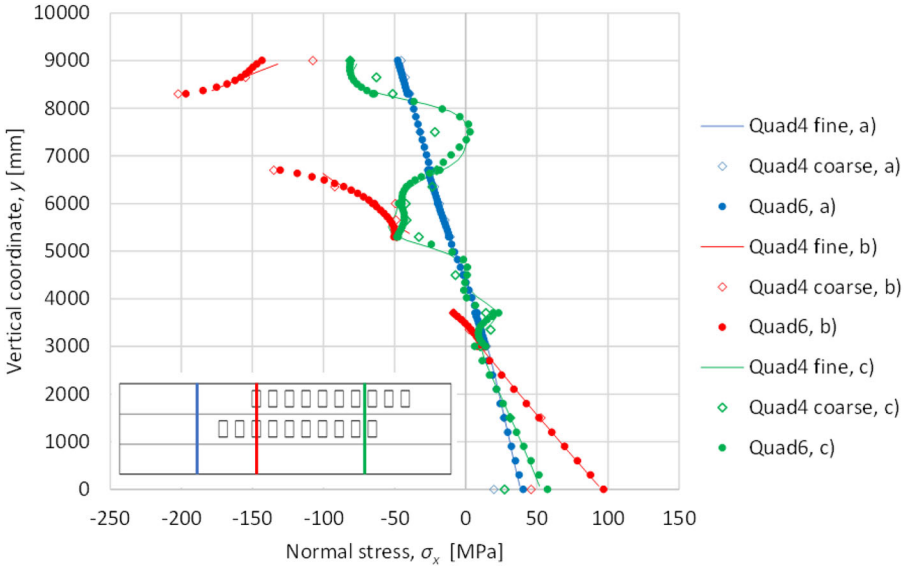

Figure 16. Vertical distribution of normal stress in cross-sections (a) x = 14,625 mm, (b) x = 24,750 mm, (c) x = 43,875 mm.

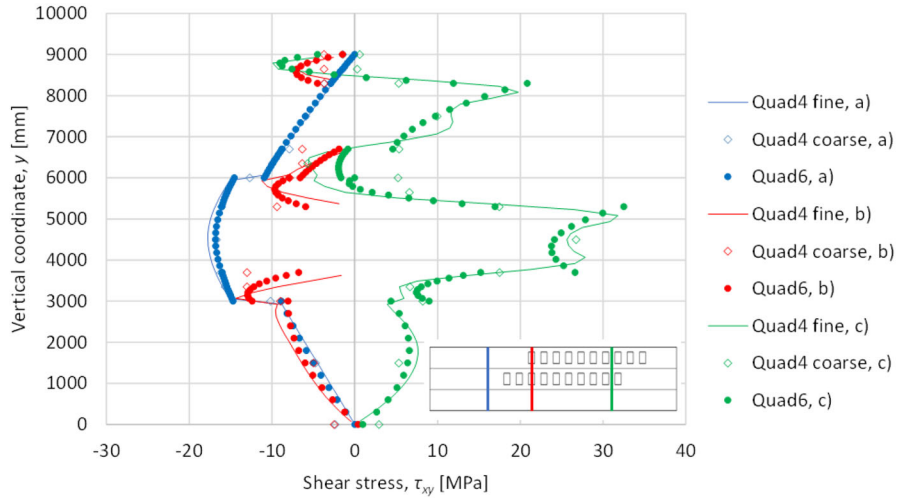

Figure 17. Vertical distribution of shear stress in cross-sections (a) x = 14,625 mm, (b) x = 24,750 mm, (c) x = 43,875 mm.

continuous structures. In real-world marine applications, these resemble hull and superstructure transitions and superstructure openings.

Simple cantilever analysis provided insight into the capabilities of the presented layerwise theory in comparison to a variety of classical theories and Carrera's unified formulations analyzed in [37] using a selection of expansion models. The presented layerwise method was highly coincident with the hierarchical Legendre expansion models presented in [37] being able to accurately describe stress behavior in a cross-section with varying stiffness regions. In addition, the formulation proved highly beneficial in problems typical for passenger ships in which stress analysis is of great importance. In areas of continuous structures, but with high stiffness variations between layers, the formulation showed excellent agreement in displacements and normal and shear stresses in comparison to the fine mesh FEA, the agreement improving with decreased element size. In the vicinity of discontinuities for stepped layers, the new formulation provides very accurate results in comparison to the fine mesh. Underestimation of peak shear stresses with the large Quad6 elements became evident in the ship height direction, in the vicinity of the layer discontinuities. However, it was shown that decreasing the element size increases the accuracy. In shear-weak regions, the new Quad6 formulation similarly provided very accurate and better results than the Quad4 coarse mesh.

In practice, this formulation allows naval architects to perform initial stress analysis of passenger ship structures with improved accuracy. The method presented in this paper serves as an alternative method for detailed 3 D FEM with good accuracy and low computational cost. In addition to the static response of structures, the lowest natural frequencies of ship structures and hull girders play a significant role in early-stage ship design. In future work, it would be beneficial to extend the method to estimate the global dynamic response of the passenger structure by continuing the work of Rehan [33]. Also, the recent non-classical continuum mechanics formulations [51] should be investigated further to define the roles of symmetric and antisymmetric

shear strain formulations more clearly in the passenger ship context.

Acknowledgments

This research work was financed by the Estonian Research Council via grant PRG83 (Numerical simulation of the FSI for the dynamic loads and response of ships). This help is gratefully appreciated.

ORCID

Hendrik Naar http://orcid.org/0000-0003-2221-7684

References

[1] T. Yao, Hull girder strength, Mar. Struct., vol. 16, no. 1, pp. 1–13, 2003. DOI: 10.1016/S0951-8339(02)00052-7.

[2] Y. Sumi, Structural safety of ships developed by lessons learned from the 100-year history of break-in-two accidents, Mar. Struct., vol. 64, pp. 481–491, 2019. DOI: 10.1016/j.marstruc.2018.12.003.

[3] H. Naar, P. Varsta, and P. Kujala, A theory of coupled beams for strength assessment of passenger ships, Mar. Struct., vol. 17, no. 8, pp. 590–611, 2004. DOI: 10.1016/j.marstruc.2005.03.004.

[4] G. Shi and D. Gao, Analysis of hull girder ultimate strength for cruise ship with multi-layer superstructures, Ships Offshore Struc., vol. 14, no. 7, pp. 698–708, 2019. DOI: 10.1080/17445302.2018.1552548.

[5] G. Shi and D. Gao, Model experiment of large superstructures' influence on hull girder ultimate strength for cruise ships, Ocean Eng., vol. 222, p. 108626, 2021. DOI: 10.1016/j.oceaneng.2021.108626.

[6] J. Romanoff, et al., Hull-superstructure interaction in optimised passanger ships, J. Ships Offshore Struct., vol. 8, no. 6, pp. 612–620, 2013. DOI: 10.1080/17445302.2012.675196.

[7] F. Morshedsoluk and M. R. Khedmati, Ultimate strength of composite ships' hull girders on the presence of composite superstructures, Thin-Walled Struct., vol. 102, pp. 122–138, 2016. DOI: 10.1016/j.tws.2016.01.024.

[8] T. Yao, et al., Ultimate Strength (Committee III.1), 16th International Ship and Offshore Structures Congress, vol. 1, 2006.

[9] E. Avi, Equivalent shell element for passenger ship structural design, Doctoral Dissertation, Aalto University, 2021.

[10] S. P. Timoshenko, History of the Strength of Materials, McGraw-Hill, New York, pp. 434–439, 1953.

[11] L. Crawford, Theory of long ships' superstructure, Trans. SNAME., vol. 58, pp. 693–732, 1950.

[12] H. H. Bleich, Nonlinear distribution of bending stresses due to distortion of the cross section, J. Appl. Mech., vol. 20, no. 1, pp. 95–104, 1953. DOI: 10.1115/1.4010600.

[13] J. Romanoff, A. T. Karttunen, P. Varsta, H. Remes, and B. R. Goncalves, A review on non-classical continuum mechanics with applications in marine engineering, Mech. Adv. Mater. Struct., vol. 27, no. 13, pp. 1065–1075, 2020. DOI: 10.1080/15376494.2020.1717693.

[14] R. Toming, E. H. Kerge, H. Naar, K. Tabri, J. Romanoff, and H. Remes, Hull and superstructure interaction using coupled beam method, Proceedings of PRADS2016, 4–8 September, Copenhagen, Denmark, pp. 851–859, 2016.

[15] H. Naar, Ultimate strength of hull girder for passenger ships, Doctoral Dissertation, Helsinki University of Technology, 2006.

[16] S. P. Timoshenko, On the correction for shear of the differential equation for transverse vibrations of prismatic bars, Philos. Mag., Ser., vol. 6, pp. 742–746, 1921. DOI: 10.1080/14786442108636264.

[17] M. Levinson, A new rectangular beam theory, J. Sound Vib., vol. 74, no. 1, pp. 81–87, 1981. DOI: 10.1016/0022-460X(81)90493-4.

[18] W. B. Bickford, A consistent higher order beam theory, Development in Theoretical and Applied Mechanics, SECTAM, vol. 11, pp. 137–150, 1982.

[19] L. W. Rehfield and P. L. N. Murthy, Toward a new engineering theory of bending, Fundam. AIAA J., vol. 20, no. 5, pp. 693–699, 1982. DOI: 10.2514/3.7938.

[20] A. V. Krishna Murty, Towards a consistent beam theory, AIAA J., vol. 22, no. 6, pp. 811–816, 1984. DOI: 10.2514/3.8685.

[21] A. Bhimaraddi and K. Chandrashekhara, Observations on higher order beam theory, J. Aerosp. Eng., vol. 6, no. 4, pp. 408–413, 1993. DOI: 10.1061/(ASCE)0893-1321(1993)6:4(408).

[22] M. H. Baluch, A. K. Azad, and M. A. Khidir, Technical theory of beams with normal strain, J. Eng. Mech., vol. 110, no. 8, pp. 1233–1237, 1984. DOI: 10.1061/(ASCE)0733-9399(1984)110:8(1233).

[23] Y. M. Ghugal and R. Sharma, A hyperbolic shear deformation theory for flexure and vibration of thick isotropic beams, Int. J. Comput. Methods, vol. 06, no. 04, pp. 585–604, 2009. DOI: 10.1142/S0219876209002017.

[24] Y. M. Ghugal and R. Sharma, A refined shear deformation theory for flexure of thick beams, Lat. Am. J. Solids Struct., vol. 8, no. 2, pp. 183–195, 2011. DOI: 10.1590/S1679-78252011000200005.

[25] J. N. Reddy, A simple higher-order theory for laminated composite plates, J. Appl. Mech., vol. 51, no. 4, pp. 745–752, 1984. DOI: 10.1115/1.3167719.

[26] E. Carrera, Historical review of Zig-Zag theories for multilayered plates and shells, Appl. Mech. Rev., vol. 56, no. 3, pp. 287–308, 2003. DOI: 10.1115/1.1557614.

[27] S. G. Lekhnitskii, Strength calculation of composite beams, Vestnik Inzhen. i Tekhnikoc., no. 9, 1935.

[28] S. A. Ambartsumian, Theory of Anisotropic Shells, NASA TTF-118, 1964.

[29] E. Reissner, On a mixed variational theorem and on a shear deformable plate theory, Int. J. Numer. Methods Eng., vol. 23, no. 2, pp. 193–198, 1986. DOI: 10.1002/nme.1620230203.

[30] A. Toledano and H. Murakami, A high-order laminated plate theory with improved in-plane responses, Int. J. Solids Struct., vol. 23, no. 1, pp. 111–131, 1987. DOI: 10.1016/0020-7683(87)90034-5.

[31] J. N. Reddy, A generalization of two-dimensional theories of laminated composite plates, Commun. Appl. Numer. Methods, vol. 3, no. 3, pp. 173–180, 1987. DOI: 10.1002/cnm.1630030303.

[32] D. H. Robbins and J. N. Reddy, Analysis of piezoelectrically actuated beams using a layer-wise displacement theory, Comput. Struct., vol. 41, no. 2, pp. 265–279, 1991. DOI: 10.1016/0045-7949(91)90430-T.

[33] J. Rehan, One-dimensional advanced beam models for marine structural applications, Doctoral thesis, Politecnico di Torino, 2017. DOI: 10.6092/polito/porto/2680980.

[34] A. Catapano, G. Giunta, S. Belouettar, and E. Carrera, Static analysis of laminated beams via a unified formulation, Compos. Struct., vol. 94, no. 1, pp. 75–83, 2011. DOI: 10.1016/j.compstruct.2011.07.015.

[35] A. J. M. Ferreira, et al., Analysis of thick isotropic and cross-ply laminated plates by generalized differential quadrature method and a Unified Formulation, Compos. B., vol. 58, pp. 544–552, 2014. DOI: 10.1016/j.compositesb.2013.10.088.

[36] M. Filippi, E. Carrera, and A. M. Zenkour, Static analyses of FGM beams by various theories and finite elements, Compos. B, vol. 72, pp. 1–9, 2015. DOI: 10.1016/j.compositesb.2014.12.004.

[37] A. Pagani, A. G. de Miguel, M. Petrolo, and E. Carrera, Analysis of laminated beams via Unified Formulation and Legendre polynomial expansions, Compos. Struct., vol. 156, pp. 78–92, 2016. DOI: 10.1016/j.compstruct.2016.01.095.

[38] E. Carrera, M. Petrolo, and P. Nali, Unified formulation applied to free vibrations finite element analysis of beams with arbitrary

section, Shock Vib., vol. 18, no. 3, pp. 485–502, 2011. DOI: 10.3233/SAV-2010-0528.

[39] E. Carrera, F. Miglioretti, and M. Petrolo, Computations and evaluations of higher-order theories for free vibration analysis of beams, J. Sound Vib., vol. 331, no. 19, pp. 4269–4284, 2012. DOI: 10.1016/j.jsv.2012.04.017.

[40] A. Pagani, M. Boscolo, J. R. Banerjee, and E. Carrera, Exact dynamic stiffness elements based on one-dimensional higher-order theories for free vibration analysis of solid and thin-walled structures, J. Sound Vib., vol. 332, no. 23, pp. 6104–6127, 2013. DOI: 10.1016/j.jsv.2013.06.023.

[41] A. Pagani and E. Carrera, Large-deflection and post-bucking analysis of laminated composite beams by Carrera Unified Formulation, Compos. Struct., vol. 170, pp. 40–52, 2017. DOI: 10.1016/j.compstruct.2017.03.008.

[42] A. Pagani, R. Augello, and E. Carrera, Frequency and mode change in the large deflection and post-buckling of compact and thin-walled beams, J. Sound Vib., vol. 432, pp. 88–104, 2018. DOI: 10.1016/j.jsv.2018.06.024.

[43] B. Wu, A. Pagani, M. Filippi, W. Q. Chen, and E. Carrera, Large-deflection and post-bukling analyses of isotropic rectangular plates by Carrera Unified Formulation, Int. J. Non Linear Mech., vol. 116, pp. 18–31, 2019. DOI: 10.1016/j.ijnonlinmec.2019.05.004.

[44] E. Carrera and E. Antona, A class of two-dimensional theories for anisotropic multilayered plates analysis, Accademia delle Scienze, 1995.

[45] E. Carrera, Evaluation of layerwise mixed theories for laminated plates analysis, AIAA J., vol. 36, no. 5, pp. 830–839, 1998. DOI: 10.2514/2.444.

[46] E. Carrera, Developments, ideas, and evaluations based upon Reissner's Mixed Variational Theorem in the modeling of multilayered plates and shells, Appl. Mech. Rev., vol. 54, no. 4, pp. 301–329, 2001. DOI: 10.1115/1.1385512.

[47] E. Carrera, M. Filippi, and E. Zappino, Free vibration analysis of rotating composite blades via Carrera Unified Formulation, Compos. Struct., vol. 106, pp. 317–325, 2013. DOI: 10.1016/j.compstruct.2013.05.055.

[48] E. Carrera and E. Zappino, Carrera unified formulation for free-vibration analysis of aircraft structures, AIAA J., vol. 54, no. 1, pp. 1–13, 2015. DOI: 10.2514/1.J054265.

[49] R. B. Bharati, M. Filippi, P. K. Mahato, and E. Carrera, Flutter analysis of llaminated composite structures using Carrera Unified Formulation, Compos. Struct., vol. 253, no. 1, p. 112759, 2020. DOI: 10.1016/j.compstruct.2020.112759.

[50] A. Pagani and E. Carrera, Unified formulation of geometrically nonlinear refined beam theories, Mech. Adv. Mater. Struct., vol. 25, no. 1, pp. 15–31, 2018. DOI: 10.1080/15376494.2016.1232458.

[51] E. Carrera and V. V. Zozulya, Carrera unified formulation (CUF) for the micropolar beams: Analytical solutions, Mech. Adv. Mater. Struct., vol. 28, no. 6, pp. 583–607, 2021. DOI: 10.1080/15376494.2019.1578013.